

## Article

# Effect of Oxygen Content on the Properties of Sputtered TaO<sub>x</sub> Electrolyte Film in All-Solid-State Electrochromic Devices

Jiuyong Li <sup>1,2</sup> , Weiming Liu <sup>1,2</sup>, Youxiu Wei <sup>1,2</sup> and Yue Yan <sup>1,2,\*</sup><sup>1</sup> Beijing Institute of Aeronautical Materials, Beijing 100095, China<sup>2</sup> Beijing Engineering Research Center of Advanced Structural Transparencies to the Modern Traffic System, Beijing 100095, China

\* Correspondence: yue.yan@biam.ac.cn

**Abstract:** Tantalum oxide (TaO<sub>x</sub>) thin films are one of the commonly used solid electrolytes in inorganic all-solid-state electrochromic devices (ECDs). The chemical composition and microstructure of TaO<sub>x</sub> films have a crucial influence on its electron blocking and ion transport properties in all-solid-state ECDs. In this work, various oxygen flux was used to deposit the TaO<sub>x</sub> films with different compositions and microstructures by pulsed direct current (p-DC) reactive magnetron sputtering. The structural properties, morphologies, chemical compositions, optical properties, electron blocking, and ionic conductive properties of the TaO<sub>x</sub> films were systematically investigated. The results show that in a certain range, the higher the oxygen flux, the stronger the ion transport ability of TaO<sub>x</sub> and the lower the electronic conductivity, which could be attributed to the loose structure and smaller number of oxygen vacancies of the films, respectively. Moreover, an all-solid-state ECD with the multilayer structure of glass/ITO/WO<sub>3</sub>/Li/TaO<sub>x</sub>/NiO/ITO was also fabricated by the magnetron sputtering method. The device exhibited excellent comprehensive electrochromic properties including high optical modulation, large coloring efficiency, fast response (especially bleaching process), and good cycle stability.



**Citation:** Li, J.; Liu, W.; Wei, Y.; Yan, Y. Effect of Oxygen Content on the Properties of Sputtered TaO<sub>x</sub> Electrolyte Film in All-Solid-State Electrochromic Devices. *Coatings* **2022**, *12*, 1831. <https://doi.org/10.3390/coatings12121831>

Academic Editor: Marcello Campajola

Received: 25 October 2022

Accepted: 23 November 2022

Published: 26 November 2022

**Publisher's Note:** MDPI stays neutral with regard to jurisdictional claims in published maps and institutional affiliations.



**Copyright:** © 2022 by the authors. Licensee MDPI, Basel, Switzerland. This article is an open access article distributed under the terms and conditions of the Creative Commons Attribution (CC BY) license (<https://creativecommons.org/licenses/by/4.0/>).

**Keywords:** tantalum oxide; solid electrolyte; magnetron sputtering; all-solid-state; electrochromic device; ion conducting layer

## 1. Introduction

Electrochromic devices (ECDs) can reversibly and permanently change optical properties such as transmittance, absorptivity, and reflectivity under an applied external voltage, which is manifested as color change in appearance. Due to their large optical modulation, relatively low driving voltage, and multi-band independent control, ECDs have been widely used in building windows, automotive anti-glare rearview mirrors, aircraft portholes, and other fields [1].

In general, ECDs consist of five layers: a transparent conductive (TC) layer/electrochromic layer/ electrolyte layer or ion-conducting layer/ion storage layer/TC layer [2–6]. As is well-known, WO<sub>3</sub> and NiO have been widely studied and used as an electrochromic layer and ion storage layer, respectively [2–8]. However, research on the electrolyte layer which plays an important role in conducting ions and blocking electrons in ECDs is still relatively insufficient. Among various electrolytes, inorganic solid electrolytes have attracted much attention due to their excellent weather resistance, simple preparation, and strong electrochemical and chemical stability compared with liquid or gel electrolytes [5,6,8]. Inorganic solid electrolytes mainly include H<sup>+</sup>-type electrolytes and Li<sup>+</sup>-type electrolytes. Although H<sup>+</sup>-type electrolytes have high proton mobility owing to the small size and light mass of protons, they are susceptible to environmental humidity, which restricts their practical application in all-solid-state ECDs [9]. Compared with H<sup>+</sup>-type electrolytes, Li<sup>+</sup>-type electrolytes are stable enough to withstand years of ECD operation without degradation, while maintaining the low resistance to Li<sup>+</sup> during diffusion [2].

Tantalum oxide ( $\text{TaO}_x$ ) is an inorganic solid electrolyte frequently used in all-solid-state ECDs due to its high transparency, good chemical and thermal stability, low leakage current, and good ionic conductivity [4,10,11]. However, in fact, it is used more as an  $\text{H}^+$ -type electrolyte, and there are few and immature studies on its use as a  $\text{Li}^+$ -type electrolyte. In addition, the high ionic conductivity and electronic insulation ability of the electrolyte depend on the microstructure and composition of the material, which is determined by the preparation technology and related process parameters [12–14]. For the practical application of inorganic solid electrolyte in ECDs, process compatibility and reliability are very important in the industrial manufacturing of ECDs. Reactive magnetron sputtering technology has been widely selected and used for the fabrication of all-solid-state ECDs, because it can continuously deposit each layer of ECDs without breaking the vacuum to achieve integrated preparation [5,15]. Moreover, it has a fast deposition rate, low operating temperature, and its process variables can be controlled independently.

In this work,  $\text{TaO}_x$  thin films were deposited at various oxygen flux using pulsed direct current (p-DC) reactive magnetron sputtering. Various material properties including structure, compositions, morphologies, optical, electrical, and electrochemical properties were systematically studied. The relationship between the ionic conductive and electron blocking properties as well as the microstructure and composition of  $\text{TaO}_x$  electrolyte films are discussed. Finally, an all-solid-state ECD with the configuration of glass/ITO/ $\text{WO}_3$ /Li/ $\text{TaO}_x$ /NiO/ITO was prepared using the magnetron sputtering method, in which an additional Li layer was added as an active ion source [16], and its electrochromic properties were systematically investigated.

## 2. Materials and Methods

### 2.1. Preparation of $\text{TaO}_x$ Films

The  $\text{TaO}_x$  films were prepared by p-DC reactive magnetron sputtering (Technol, Beijing, China) from a Ta target ( $\Phi 74.5 \text{ mm} \times 4.6 \text{ mm}$ ) at room temperature. Silica glass and ITO/ $\text{WO}_3$ -coated glass were used as the substrates. The  $\text{TaO}_x$  films sputtered on silica glass substrates were used as a physical characterization, and  $\text{TaO}_x$  sputtered on ITO/ $\text{WO}_3$ -coated glass substrates were used as ion transport performance measurements. The target-to-substrate distance was approximately 10 cm. Prior to the deposition, silica glass substrates were ultrasonically cleaned in absolute ethanol and deionized water for 10 min and blown dried with  $\text{N}_2$ . The chamber was vacuumized to a base pressure of  $1 \times 10^{-3} \text{ Pa}$  and the Ta target was pre-sputtered in a pure argon atmosphere for 10 min to remove the surface contaminations. During deposition, the total pressure was kept at 1.2 Pa and the sputtering power was maintained at 120 W. The  $\text{TaO}_x$  films with different oxygen content were obtained by adjusting oxygen flux, and the Ar/ $\text{O}_2$  gas flow ratio was 30/2, 30/2.5, 30/3, 30/4, and 30/5 (unit: sccm). The substrate kept rotating at a speed of 6 rpm to guarantee film uniformity during the sputtering. The angle between the target surface and the substrate is about  $35^\circ$ .

### 2.2. Preparation of All-Solid-State ECD

The inorganic all-solid-state ECDs (glass/ITO/ $\text{WO}_3$ /Li/ $\text{TaO}_x$ /NiO/ITO) were individually prepared layer by layer on ITO-coated glass ( $\sim 7 \Omega/\square$ ) by magnetron sputtering at room temperature. The ITO-coated glass will be ultrasonically cleaned in absolute ethanol and deionized water for 10 min and blown dried with  $\text{N}_2$  before preparation. The preparation of each layer was carried out continuously in a multi-target magnetron sputtering system. Each target ( $\Phi 74.5 \text{ mm}$ ) was equipped with a cover in order to avoid cross-contamination. Pre-sputtering was performed in an Ar gas flow of 30 sccm for 10 min before each layer deposition. The base pressure of the chamber was vacuumized to  $1 \times 10^{-3} \text{ Pa}$ . The target-to-substrate distance was about 10 cm. The substrate stage kept rotating to obtain uniform films. Ar (99.999%),  $\text{O}_2$  (99.999%), and Ar- $\text{O}_2$  mixture gas (90% Ar + 10%  $\text{O}_2$ , 99.999%) were used, and their flow rates were adjusted by mass flow controllers. Among them, Ar- $\text{O}_2$  mixture gas was selected instead of  $\text{O}_2$  for the prepared of

NiO and ITO films to ensure the accurate ratio of argon to oxygen owing to the low amount of O<sub>2</sub> required for deposition. The detailed deposition parameters for WO<sub>3</sub>, NiO, Li, TaO<sub>x</sub>, and top ITO layers are listed in Table 1.

**Table 1.** Deposition parameters for the WO<sub>3</sub>, NiO, Li, TaO<sub>x</sub>, and top ITO layers of all-solid-state ECD.

Film	Target	Power Source	Ar: O <sub>2</sub> : Ar-O <sub>2</sub> <sup>a</sup> (sccm)	Pressure (Pa)	Sputtering Power (W)	Thickness (nm)
WO <sub>3</sub>	W	p-DC	32:8:0	1.5	120	300
NiO	Ni	p-DC	11:0:14	2	130	150
Li	Li	DC	30:0:0	0.5	60	40
TaO <sub>x</sub>	Ta	p-DC	30:4:0	1.2	120	300
ITO	ITO	DC	24.6:0:6	0.5	100	150

<sup>a</sup> Ar-O<sub>2</sub> mixture gas (90% Ar + 10% O<sub>2</sub>).

### 2.3. Physical Characterization

The structures of the TaO<sub>x</sub> films on silica glass substrates were measured by X-ray diffractometer (XRD, Bruker D8 Advance, Karlsruhe, Germany) with the X-ray of Cu K $\alpha$  radiation. The diffraction scanning 2 $\theta$  range was 10–80° with a step of 0.06° and a step time of 0.1 s. The surface morphologies and roughness of the TaO<sub>x</sub> films were analyzed by scanning electron microscope (SEM, Hitachi SU-8010, Tokyo, Japan) and atomic force microscope (AFM, Bruker Dimension, Karlsruhe, Germany). The acceleration voltage of SEM was 3 kV, and the working distance was 2–4 mm. For AFM, tapping mode was used with a scan rate of 1 Hz and a scan range of 5  $\mu$ m. The cross-sectional morphology of the ECD was also acquired by SEM and the cross-section was exposed to the air for a short time before SEM observation. The thickness of the TaO<sub>x</sub> films were measured by a surface profiler (P-7, KLA Tencor, San Francisco, CA, USA) and consisted well with the cross-sectional SEM results. The composition of the TaO<sub>x</sub> films were determined by X-ray photoelectron spectroscopy (XPS, Thermo ESCALAB 250Xi, Waltham, MA, USA). The X-ray source was monochromatic Al K $\alpha$  (h $\nu$  = 1486.6 eV). The working power was 150 W, the voltage was 14.8 kV, the current was 1.6 A, the take-off angle was 55°, and the spot diameter was 650  $\mu$ m. High-resolution scan spectra was collected at 20 eV passing energy and 0.1 eV step. Charge correction was performed by fixing the C 1 s peak at 284.8 eV. Thermo Avantage software (version 5.9918) was used to analyze the XPS data.

### 2.4. Optical and Electrochemical Measurements

The transmittance spectra of the TaO<sub>x</sub> films were collected by ultraviolet-visible-near-infrared (UV-Vis-NIR) spectrophotometer (Agilent Cary 5000, Santa Clara, CA, USA) in the wavelength range of 200–1500 nm. The transmittance spectra of the ECD in bleached and colored state were acquired in the wavelength range of 380–800 nm. The in situ transmittance change of the ECD at 550 nm over time was recorded. Air was employed as baseline in the above measurements.

The typical Au/TaO<sub>x</sub>/Au sandwich structures were served for the electronic conductivity measurements, in which the Au film was prepared by DC magnetron sputtering with a thickness of about 100 nm. The effective active electrode area was 4 mm<sup>2</sup>. The sandwich structures were applied with a DC constant voltage of 2 V, and the current was recorded.

The electrochemical properties of the films and the ECD were studied on CHI 660E electrochemical workstation (Chinstruments, Shanghai, China) at room temperature. Electrochromic behaviors of the TaO<sub>x</sub>-coated ITO/WO<sub>3</sub> electrodes were investigated by Chronocoulometry (CC) with in situ transmittance recording, and a standard three-electrode system was carried out containing 0.1 M LiClO<sub>4</sub>-PC (propylene carbonate) as the electrolyte, TaO<sub>x</sub>-coated ITO/WO<sub>3</sub> as the working electrode, Ag/AgCl as the reference electrode, and platinum foil as the counter electrode. In the CC measurement, the TaO<sub>x</sub>-coated ITO/WO<sub>3</sub> electrodes were colored at −1 V and bleached at 1 V, and the duration was 30 s. The electrochemical measurements of the ECD were carried out with a two-electrode system,

where the bottom ITO layer close to  $\text{WO}_3$  layer was employed as the working electrode and the top ITO layer adjacent to NiO layer was used as the reference and counter electrodes. The EC properties of the ECD were measured based on step chronoamperometry (CA) and cyclic voltammetry (CV). The cycling stability of the as-prepared ECD were measured by CA for 1000 cycles. The applied voltage and duration were  $-1.5$  V for 40 s (coloration) and 1 V for 20 s (bleaching) in CA cycles. The CV measurements were performed between  $-1.5$  V and 1 V at a scan rate of  $50 \text{ mV s}^{-1}$ .

### 3. Results and Discussion

#### 3.1. Determination of the $\text{TaO}_x$ Deposition Conditions

The hysteresis curve of target voltage vs. oxygen flux of  $\text{TaO}_x$  thin films was measured and recorded to choose suitable deposition conditions, as shown in Figure 1. With the gradual increase in oxygen flux, the target voltage first rises rapidly and then slows down. When the oxygen flux exceeds 5 sccm, the target voltage remains substantially constant, indicating that the Ta target surface has been sufficiently oxidized and almost covered by tantalum oxide [17]. As the oxygen flux drops from 6 sccm to 0 sccm, the target voltage decreases and a narrow hysteresis region is formed between 2–4 sccm. When the oxygen flux is lower than 1 sccm, the deposited film is mainly metal state [4,17]. The change trend of target voltage with oxygen flux during the reactive magnetron sputtering of the  $\text{TaO}_x$  thin films is related to the emitted secondary electrons of target surface components [18]. The  $\text{Ta}_2\text{O}_5$  component on the target surface increases with the increase in oxygen flux based on the Berg's model [19], which will result in the decrease in total emitted secondary electrons due to the smaller secondary electron emission coefficient of  $\text{Ta}_2\text{O}_5$ . Consequently, the current decreases and target voltage increases under the constant power mode [4]. Finally, based on the hysteresis curve, the oxygen flux range is determined to be 2–5 sccm. The deposition rates under the selected deposition conditions were also measured, as shown in Figure 1. As the oxygen flow exceeds 2.5 sccm, the deposition rate is rapidly decreased since the target surface oxide layer gradually increases, and when the oxygen flux reaches 5 sccm, the deposition rate is only  $4 \text{ nm min}^{-1}$ .

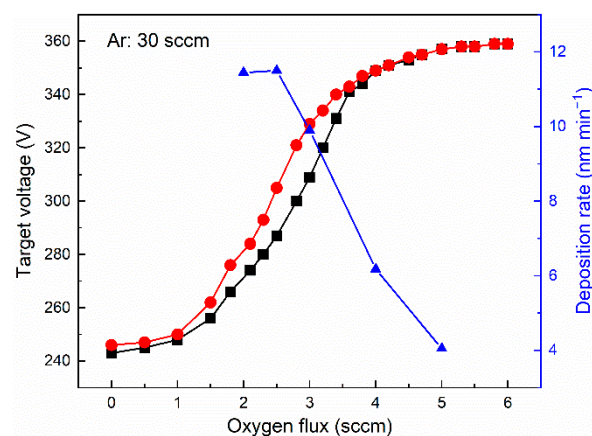


**Figure 1.** The relationship curves of target voltage and deposition rate vs.  $\text{O}_2$  flux during reactive magnetron sputtering for preparation of  $\text{TaO}_x$  thin films. (Black line is the target voltage change when oxygen flux rate increases, red line is the target voltage change when oxygen flux decreases, and blue line is deposition rate).

#### 3.2. Structure, Morphology, Composition, and Optical Properties of the $\text{TaO}_x$ Thin Films

In order to determine the crystal structure of the  $\text{TaO}_x$  thin films, XRD measurements were carried out. As shown in Figure 2, no diffraction peaks are detected by XRD in  $2\theta$  range of  $10$ – $80^\circ$ , and the broad humps between  $15$ – $25^\circ$  originate from the silica glass substrates. All  $\text{TaO}_x$  films are amorphous regardless of Ar/ $\text{O}_2$  ratio. This demonstrates

that TaO<sub>x</sub> films sputtered at room temperature or low substrate temperature are difficult to crystallize.

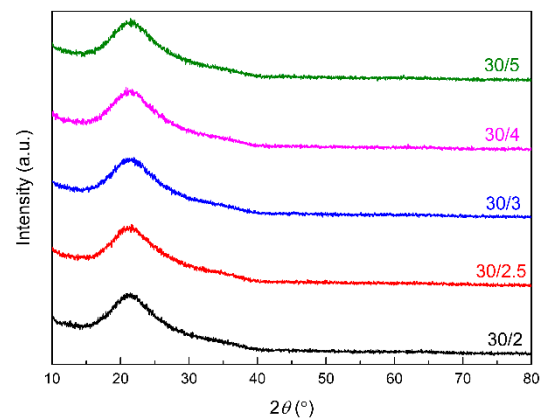


**Figure 2.** XRD patterns of the TaO<sub>x</sub> films with different Ar/O<sub>2</sub> ratio deposited on silica glass substrates.

The surface and cross-sectional morphologies of the TaO<sub>x</sub> films are shown in Figure 3. The TaO<sub>x</sub> particle clusters on the surface of the film are evenly distributed. As the oxygen flux increases, the particle clusters on the surface gradually become plump, and the size is gradually increased. Further, clear cavity (void) boundaries between the particle clusters are observed with an increase in oxygen flux, and the cavities between the clusters have gradually become obvious. This probably means that the film packing density is gradually decreased. The cavities would generate a large number of surfaces and surface defects, creating the space-charge regions that could facilitate the transport of lithium ions on the surface of electrolyte film [20]. Moreover, the cross-sectional view of films show that TaO<sub>x</sub> is grown in a columnar structure, and with the increase in oxygen content, the amount of cavities between the columnar grains increases and the film structure becomes more loose.

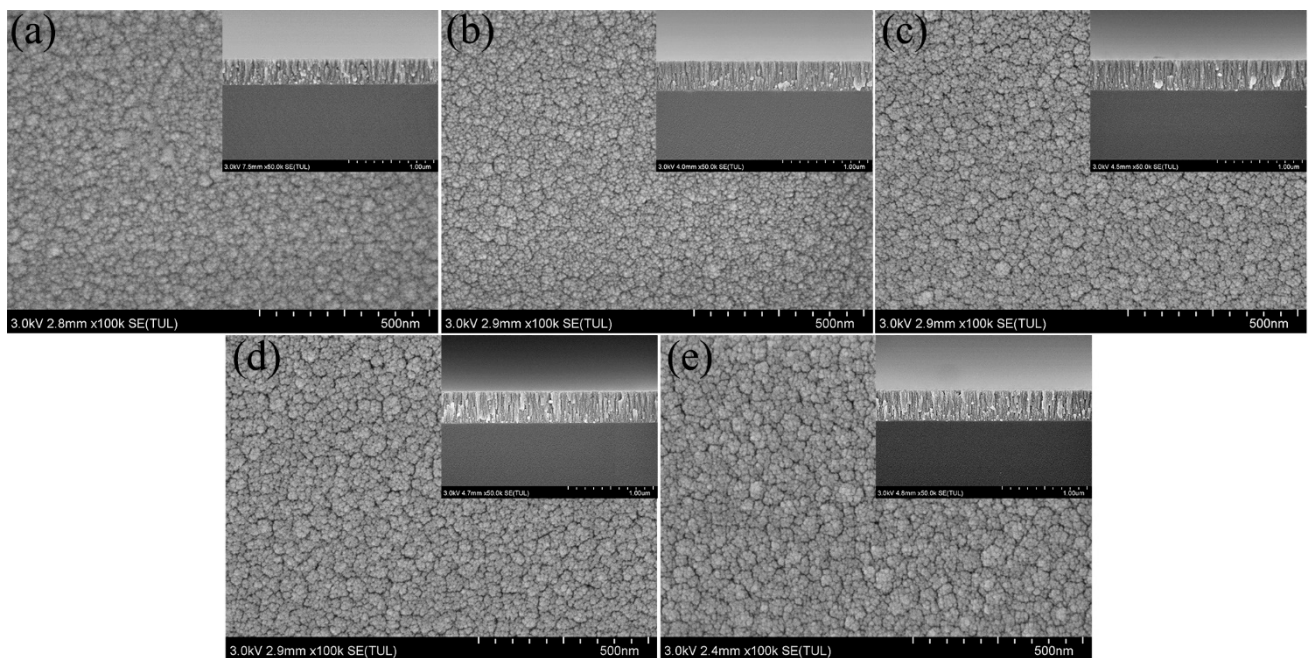


**Figure 3.** The surface and cross-sectional morphologies of the TaO<sub>x</sub> films with various Ar/O<sub>2</sub> ratio, (a) 30/2, (b) 30/2.5, (c) 30/3, (d) 30/4, and (e) 30/5.

To further characterize the surface morphology and roughness of the TaO<sub>x</sub> films, we conducted AFM measurements. Figure 4 displays AFM images of the TaO<sub>x</sub> thin films and the change trend of its roughness with various Ar/O<sub>2</sub> ratios. The particle distribution on all TaO<sub>x</sub> film surfaces is uniform, which is in accordance with the SEM results. As the oxygen flux increases, the undulation of surface particles is gradually increased, and the bright spots representing particles or clusters in Figure 4a–e becomes larger, implying that its size gradually increases. Figure 4f shows the change trend of the root mean square roughness and the average roughness of the TaO<sub>x</sub> films as the Ar/O<sub>2</sub> ratio. It can be seen that with an increase in oxygen flux, the film roughness is gradually increased. However, the overall increase is small, and all films roughness is less than 2 nm. This indicates that the flatness of the surface of the TaO<sub>x</sub> films is high, which is advantageous for uniform deposition of subsequent films in full devices.

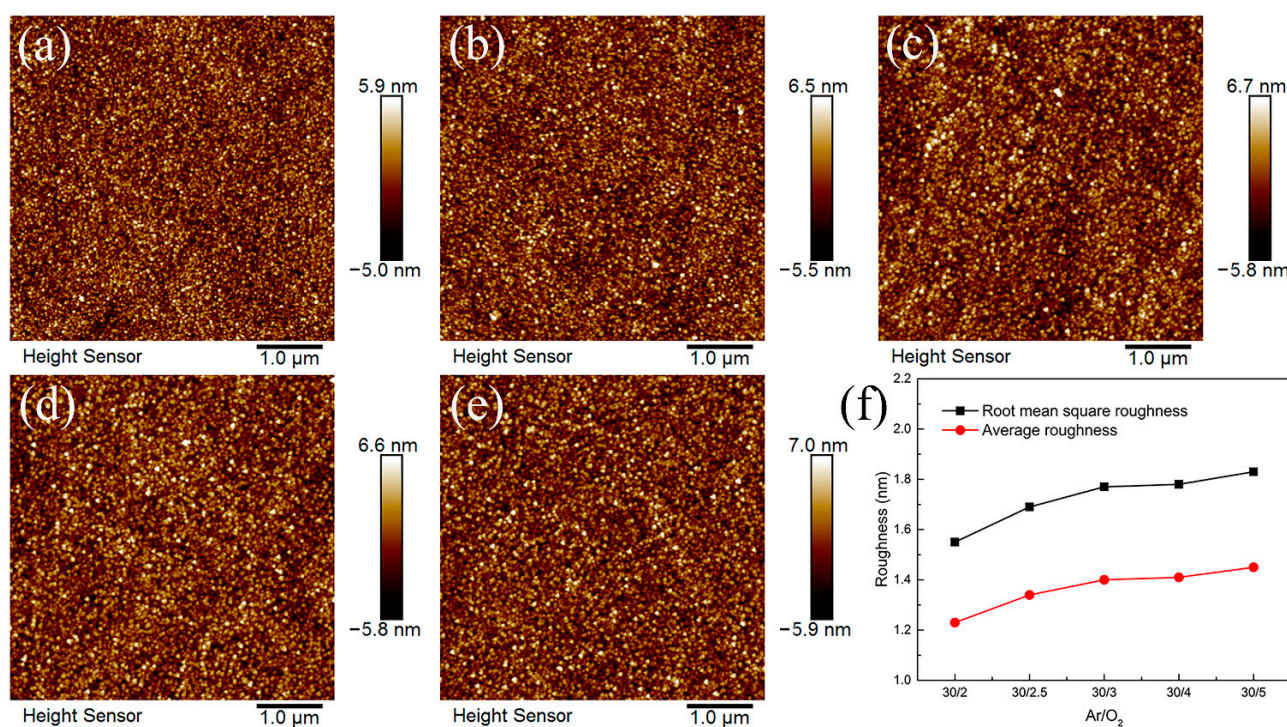


**Figure 4.** AFM images of the TaO<sub>x</sub> films with various Ar/O<sub>2</sub> ratio, (a) 30/2, (b) 30/2.5, (c) 30/3, (d) 30/4, (e) 30/5, and (f) change trend of roughness of TaO<sub>x</sub> films.

The XPS data of TaO<sub>x</sub> films sputtered with various Ar/O<sub>2</sub> ratio were collected to investigate the stoichiometry of the films. Figure 5 presents the high-resolution scan spectra of Ta 4f and O 1s for the TaO<sub>x</sub> thin films deposited with various Ar/O<sub>2</sub> ratio. As shown in Figure 5a, the binding energies of Ta4f<sub>7/2</sub> and Ta4f<sub>5/2</sub> doublet peaks were  $26.2 \pm 0.1$  eV and  $28.1 \pm 0.1$  eV, respectively, due to spin orbit splitting of the Ta<sup>5+</sup> ion nanostructure. The binding distance of both peaks for all TaO<sub>x</sub> thin films deposited with different Ar/O<sub>2</sub> ratios is kept at about 1.9 eV. Figure 5b shows that all O 1s curves could be fitted to two Gaussian peaks, in which the shoulder peak in the higher binding energy range originates from surface-adsorbed oxygen species [4,21]. The strong peak at the binding energy of  $530.4 \pm 0.1$  eV corresponds to the characteristic peak of O<sup>2-</sup> anions in TaO<sub>x</sub> films [4]. It is worth mentioning that the binding energy positions of both Ta 4f and O<sup>2-</sup> gradually move to the lower binding energy region with the increase in O<sub>2</sub> flux in the preparation of TaO<sub>x</sub> thin films. This phenomenon could be assigned to the downward shift of Fermi level caused by the decrease in oxygen vacancy concentration with the increase in O<sub>2</sub> flux [21]. Moreover, according to the peak areas of Ta 4f and O<sup>2-</sup>, the atomic ratios of O/Ta in TaO<sub>x</sub> films prepared at various Ar/O<sub>2</sub> ratio can be estimated and have been summarized in Table 2. All the prepared films were non-metallic in appearance, and the atomic ratio of

O/Ta increases with the increase in oxygen flux. The O/Ta atomic ratios of TaO<sub>x</sub> films deposited at Ar/O<sub>2</sub> ratio of 30/4 and 30/5 are close to 2.5 as that of stoichiometric Ta<sub>2</sub>O<sub>5</sub>.

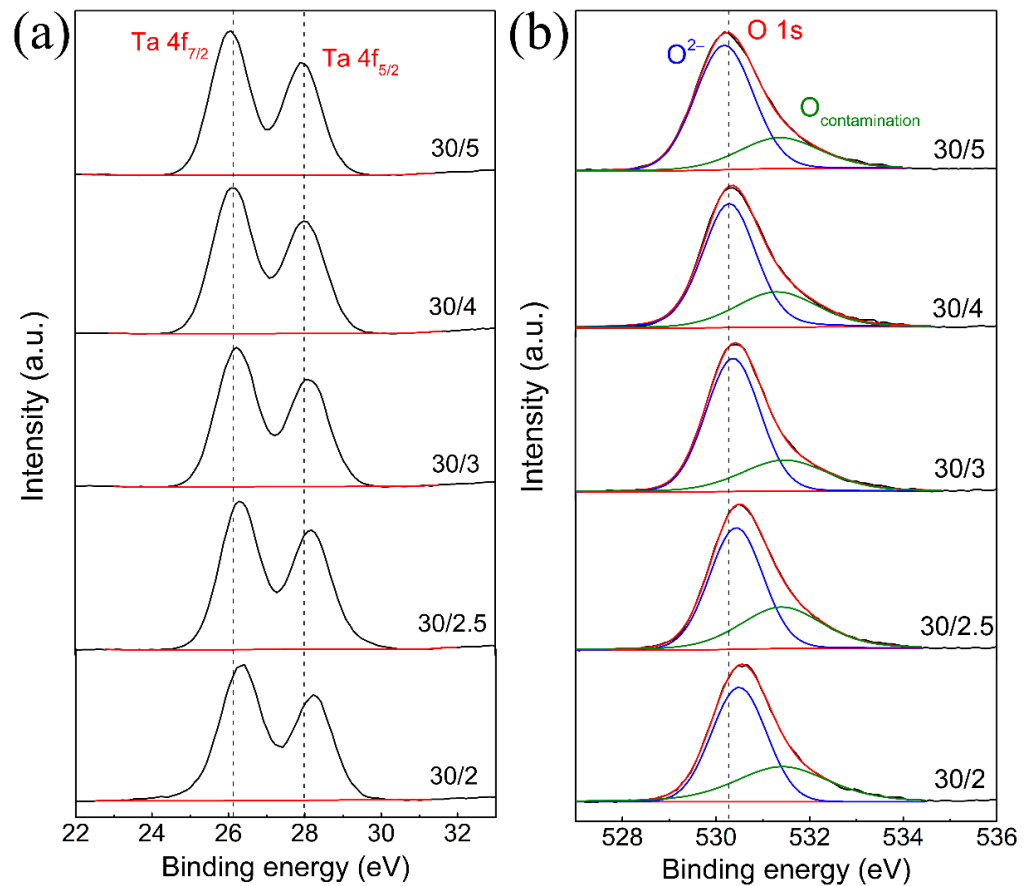


**Figure 5.** The XPS spectra of (a) Ta 4f and (b) O1 s for the TaO<sub>x</sub> thin films sputtered with various Ar/O<sub>2</sub> ratio.

**Table 2.** Summary of the XPS results for TaO<sub>x</sub> film deposited by various Ar/O<sub>2</sub> ratio.

Ar/O <sub>2</sub>	30/2	30/2.5	30/3	30/4	30/5
O at. %	67.94	68.85	69.92	71.08	71.34
Ta at. %	32.06	31.15	30.08	28.92	28.66
O/Ta	2.12	2.21	2.32	2.46	2.49

In order to characterize the optical properties of TaO<sub>x</sub> thin films sputtered with various Ar/O<sub>2</sub> ratio, the transmittance spectra of TaO<sub>x</sub> thin films deposited on silica substrates in the wavelength range of 200–1500 nm was measured, as shown in Figure 6a. High transparency in the Vis-NIR region is preferred for the electrolyte layer of ECDs. From the inset photo of Figure 6a, one can see a lesser oxygen flux, darker film color, and lower corresponding optical transmittance, which probably means that the films were not completely oxidized under low oxygen flux. When the oxygen flux exceeds 3 sccm, the transmittance of the films is relatively high. And the visible light transmittance of the films deposited from 30/2 to 30/5 is 57.7%, 72.9%, 84.4%, 85.8%, and 85.2%, respectively, which is calculated out by Equation (1) according to ISO 9050 [22]. All the films exhibit strong absorption below 300 nm.

$$\tau_v = \frac{\int_{380}^{780} D_\lambda \cdot \tau(\lambda) \cdot V(\lambda) \cdot \Delta\lambda}{\int_{380}^{780} D_\lambda \cdot V(\lambda) \cdot \Delta\lambda} \tag{1}$$

where  $\tau_v$  is the visible light transmittance,  $D_\lambda$  is the relative spectral power distribution of standard illuminant  $D_{65}$ ,  $\tau(\lambda)$  is the transmittance of film at the wavelength of  $\lambda$ ,  $V(\lambda)$  is the spectral luminous efficiency of bright vision, and  $\Delta\lambda$  is the wavelength interval, here 10 nm.

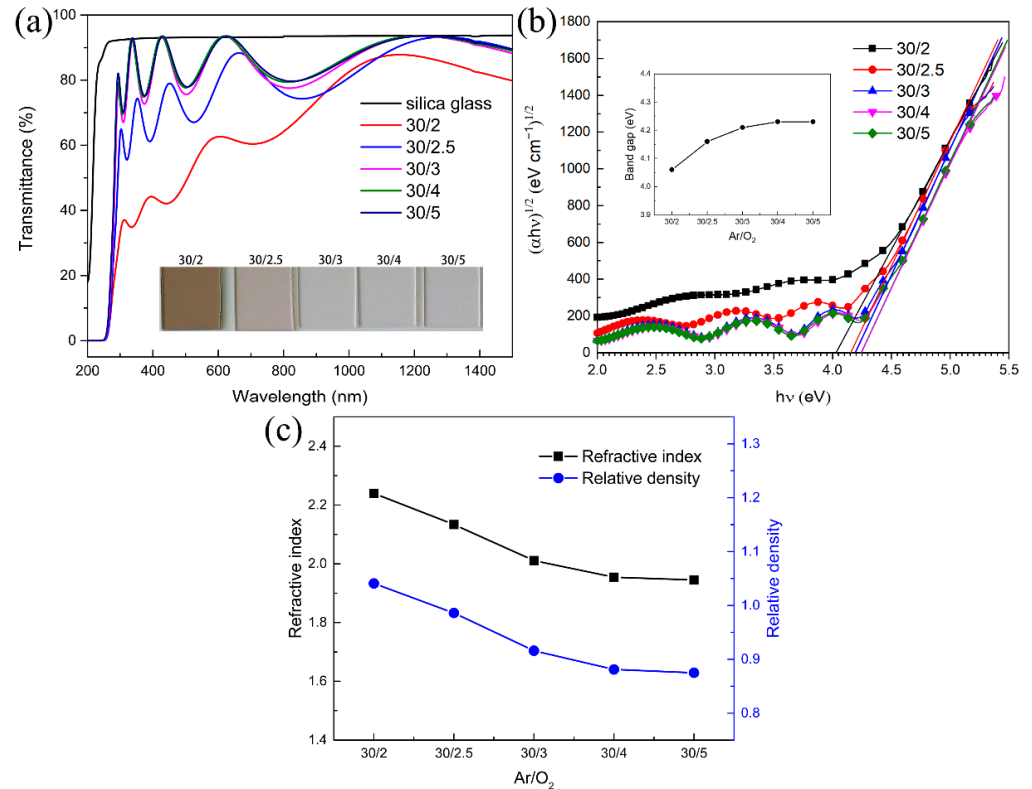


**Figure 6.** (a) Optical transmittance spectrum of the TaO<sub>x</sub> films sputtered with various Ar/O<sub>2</sub> ratio on silica glass, insert: the digital images of as-deposited films. (b)  $(\alpha h\nu)^{1/2}$  vs.  $h\nu$  plots of the TaO<sub>x</sub> films on silica glass, insert: the variation of band gap values for TaO<sub>x</sub> films. (c) The variation of refractive index and relative density of the TaO<sub>x</sub> films with different Ar/O<sub>2</sub> ratio.

Figure 6b presents the plot of  $(\alpha h\nu)^{1/2}$  versus  $h\nu$ . The optical band gaps of TaO<sub>x</sub> films with different Ar/O<sub>2</sub> ratio is estimated by the intercept of  $(\alpha h\nu)^{1/2}$  vs  $h\nu$  plot. The  $\alpha$  is optical absorption coefficient. It can be calculated by the formula  $\alpha = (-1/d) \ln(1/T)$ , where  $d$  is the thickness of the film and  $T$  is transmittance of the film. For indirect semiconductors like tantalum oxide, the dependence of the absorption coefficient on the incident photon energy ( $h\nu$ ) is given by  $(\alpha h\nu)^{1/2} = \beta (h\nu - E_g)$  [23], where  $\beta$  is a constant and  $E_g$  is the optical band gap. The band gap values are determined by extrapolating the linear regions of the plots to the  $x$ -axis ( $\alpha = 0$ ). According to the transmittance spectrum in Figure 6a, the band gap values for TaO<sub>x</sub> films were calculated to be from 4.06 to 4.23 eV with an increase in oxygen flux from 2 to 5 sccm, respectively, as shown in the insert of Figure 6b. The increase in the band gap with the increase in oxygen flux could be attributed to the different level of oxygen vacancies presented in the films. Typically, the oxygen vacancies induced by insufficient oxygen flux results in the formation of a defect band below the conduction band and thus causes a decrease in the band gap [21,24]. Owing to the lower oxygen vacancy concentrations, the larger band gap value of 4.23 eV can be obtained for the TaO<sub>x</sub> films prepared at the Ar/O<sub>2</sub> ratio of 30/4 and 30/5 compared with other films.

The refractive index ( $n$ ) of the films was determined from the optical transmittance interference data employing Swanepoel's envelope method [25] using the relations  $n(\lambda) = [N + (N^2 - n_0^2 n_1^2)^{1/2}]^{1/2}$  and  $N = 2 n_0 n_1 [(T_{\max} - T_{\min})/T_{\max} T_{\min}] + (n_0^2 + n_1^2)/2$ , where  $n_0$  and  $n_1$  are the refractive indices of air and substrate, and  $T_{\max}$  and  $T_{\min}$  are the successive optical transmittance maxima and minima, respectively. Then,

the refractive index data are used to calculate the relative density of the films using the Lorentz–Lorenz relationship [26], i.e.,  $P = (\rho_f/\rho_b) = [(n_f^2 - 1)/(n_f^2 + 2)][(n_b^2 + 2)/(n_b^2 - 1)]$ , where  $\rho_f$ ,  $\rho_b$  are the film and bulk density for Ta<sub>2</sub>O<sub>5</sub> films,  $n_b = 2.16$  is the bulk refractive index at 550 nm, and  $n_f$  is the film refractive index [27]. The variation of refractive index and relative density of TaO<sub>x</sub> thin films with Ar/O<sub>2</sub> ratio are shown in Figure 6 c. As the oxygen flux increases, the film refractive index and relative density gradually decrease, indicating that the porosity of the film is gradually increased, which is consistent with the SEM results in Figure 3. The cavities, pores, and gaps in the TaO<sub>x</sub> films deposited at high oxygen flux reduce their intrinsic refractive index, and a large number of surfaces generated may promote the conduction of Li ions by surface and result in enhanced ion transport ability [10,20].

### 3.3. Electrochemical Properties of the TaO<sub>x</sub> Films

Fast conducting ions and effective blocking electrons are the main functions of the electrolyte layer in all-solid-state ECDs. First, in order to characterize the electron blocking ability of the TaO<sub>x</sub> electrolyte layer, current–time curves of TaO<sub>x</sub> films sputtered with various Ar/O<sub>2</sub> ratio were measured by applying a DC voltage of 2 V, as shown in Figure 7. As observed, the current of all TaO<sub>x</sub> films decreases rapidly at the initial stage and then tends to be stable. The current in the initial stage originates from the polarization process of H<sup>+</sup> ionized by trace water in the air adsorbed by the film. Further, the steady-state current is owing to the electron leakage current, from which the electronic conductivity can be determined. The electronic conductivity  $\sigma_e$  can be calculated from  $\sigma_e = d/(R \times S)$  and  $R = U/I$ , where  $d$  is the thickness of the film and  $S$  is the area of the effective electrode region. It can be clearly observed that as the oxygen flux increases, the steady-state current of the sample gradually decreases, that is, the electronic conductivity gradually decreases. Studies have shown that there are a large number of oxygen vacancies in non-stoichiometric TaO<sub>x</sub> films, which form a defect band and produce an electron leakage current [28,29]. Therefore, the higher the oxygen flux in the preparation process, the higher the oxidation degree of TaO<sub>x</sub> films, and the lower its electronic conductivity. The electronic conductivities of the films deposited from 30/2 to 30/5 are  $2.06 \times 10^{-7}$ ,  $7.05 \times 10^{-11}$ ,  $1.31 \times 10^{-11}$ ,  $4.16 \times 10^{-12}$  and  $3.08 \times 10^{-12}$  S cm<sup>-1</sup>, respectively. The electronic conductivity of TaO<sub>x</sub> films prepared at 30/4 and 30/5 is very close due to their almost identical O/Ta atomic ratio. In addition, their values are comparable to the results of Li<sub>2.5</sub>TaO<sub>x</sub> electrolyte films used in a similar all-solid-state ECD structure [5]. It should be mentioned that the duration of current–time curves at a constant voltage was limited within 180 s in this measurement. Further, this polarization measurement does not provide accurate results because of the ionic space charge at the electrode/electrolyte interface [5]. The real electronic conductivities should be lower than these values.

Then, in order to study and analyze the ion transport ability of TaO<sub>x</sub>, TaO<sub>x</sub> films with different Ar/O<sub>2</sub> ratio were deposited on ITO/WO<sub>3</sub>-coated glass, and the electrochemical properties of ITO/WO<sub>3</sub>/TaO<sub>x</sub> were investigated. Figure 8 shows the CC curves and the corresponding change of in situ transmittance of ITO/WO<sub>3</sub>/TaO<sub>x</sub>, in which ITO/WO<sub>3</sub> is also measured as a control. As shown in Figure 8a, with the increase in oxygen flux, the charge capacity of the sample increases significantly, especially between 30/2.5 and 30/3. This indicates that Li ions transport more easily in TaO<sub>x</sub> films prepared at higher oxygen flux, which could be attributed to the loose structure and low relative density of the TaO<sub>x</sub> films (Figures 3 and 6c), providing a large number of surfaces for ion conduction [20]. When the oxygen flux further increases, the increase in charge capacity gradually becomes slow because the relative density of the films tends to be stable (Figure 6c). Figure 8b presents that the optical modulation (difference between colored transmittance and bleached transmittance) of the sample gradually increases with the increase in oxygen flux, which is consistent with the change of charge capacity. The larger optical modulations were obtained in the samples prepared at 30/4 and 30/5 Ar/O<sub>2</sub> ratios, which were 63.3% and 65.5%, respectively. It should be noted that the transmittance of deposited state (or bleached

state) TaO<sub>x</sub> sample with Ar/O<sub>2</sub> ratio of 30/2 is low. This is because the insufficient amount of oxygen makes TaO<sub>x</sub> in a severe anoxic state, reducing WO<sub>3</sub> in the lower layer (reducing W<sup>6+</sup> to W<sup>5+</sup>), resulting in a blue color of the deposited sample—that is, a low transmittance.

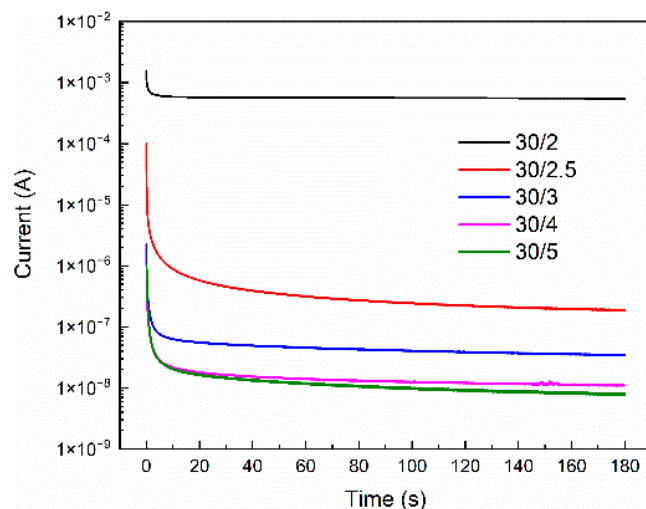


**Figure 7.** Current–time curves of TaO<sub>x</sub> films sputtered with various Ar/O<sub>2</sub> ratio under a DC voltage of 2 V.

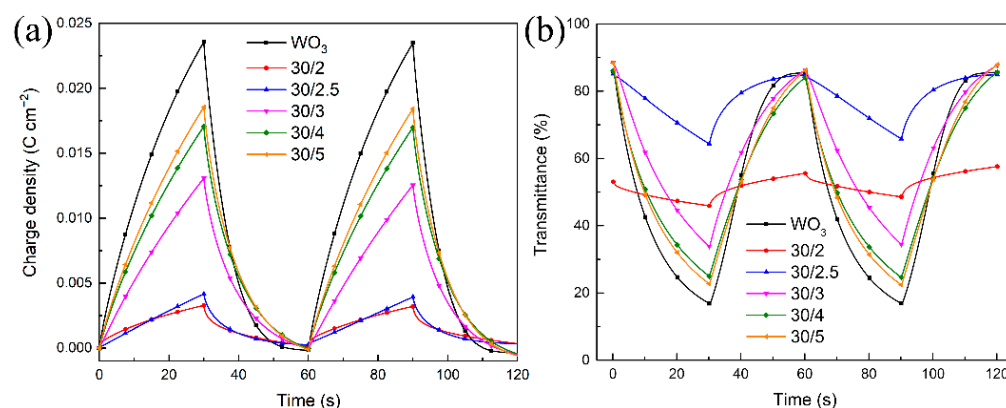


**Figure 8.** The variation of CC curves (a) and the corresponding transmittance (b) of ITO/WO<sub>3</sub>/TaO<sub>x</sub> with different Ar/O<sub>2</sub> ratios.

### 3.4. Characterization of the All-Solid-State ECD

The above results show that the increase in oxygen flux will decrease the relative density of the films and reduce oxygen vacancies, which, to some extent, is conducive to the enhancement of ion conduction ability and the reduction in electronic conductivity of TaO<sub>x</sub>, respectively. The TaO<sub>x</sub> films deposited at the Ar/O<sub>2</sub> ratio of 30/4 and 30/5 have similar ion transport ability and electronic barrier properties due to their close relative density and O/Ta atomic ratio. In addition, it is worth emphasizing that the TaO<sub>x</sub> film with 30/4 has a faster deposition rate of 6.2 nm min<sup>−1</sup> (Figure 1), which is 1.55 times that of the TaO<sub>x</sub> film with 30/5. Therefore, the TaO<sub>x</sub> film with Ar/O<sub>2</sub> ratio of 30/4 was selected and prepared as the electrolyte layer in the fabrication of inorganic all-solid-state ECD.

The structural schematic diagram of the all-solid-state ECD corresponding to deposition sequence is illustrated in Figure 9a. Li is sputtered after the deposition of the WO<sub>3</sub> layer, and it cannot be detected because Li diffuses directly into the WO<sub>3</sub> layer to reduce it to blue Li<sub>x</sub>WO<sub>3</sub> (Figure S1) [30]. Cross-sectional morphology of the ECD presented in Figure 9b clearly shows a five-layer structure ITO/Li<sub>x</sub>WO<sub>3</sub>/TaO<sub>x</sub>/NiO/ITO (Li has diffused into WO<sub>3</sub> layer). The interfaces between the layers can be clearly identified, suggesting that these layers are chemically and physically stable [2]. The thickness of each layer from top

to bottom is approximately 250 nm, 150 nm, 300 nm, 300 nm, and 250 nm, respectively. This is in accordance with the predicted value. In addition, the XRD patterns of  $\text{WO}_3$ ,  $\text{WO}_3/\text{Li}$  and  $\text{NiO}$  films were also measured and displayed in Figure S2, indicating that the  $\text{WO}_3$  and  $\text{WO}_3/\text{Li}$  films are amorphous and  $\text{NiO}$  is a face-centered cubic structure.

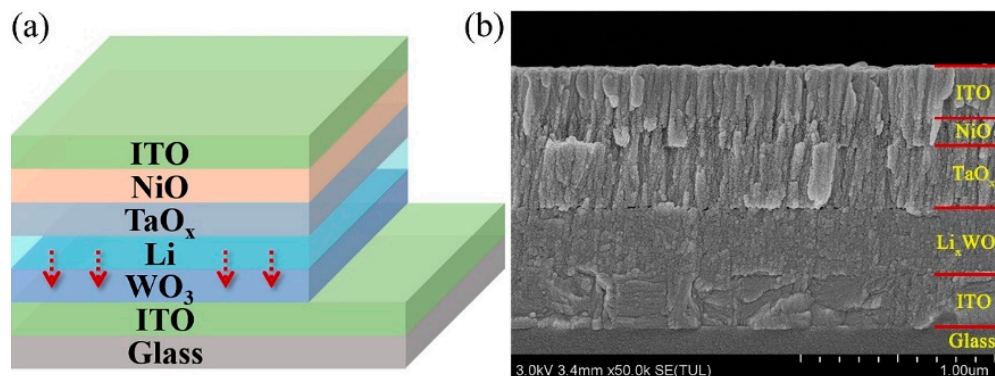


**Figure 9.** Structural schematic diagram (a) and cross-sectional morphology (b) of the all-solid-state ECD. (Arrow represents Li diffusion into  $\text{WO}_3$  layer).

The electrochemical characteristics and electrochromic performance of the ECD were investigated by CV and transmittance measurements. Figure 10a displays the CV curves of the ECD after 10 cycles and 1000 cycles in the voltage range of  $-1.5$  to  $1$  V at a scan rate of  $50 \text{ mV s}^{-1}$ . It is found that the features of CV curves are similar to those of single  $\text{WO}_3$  film, which indicates that  $\text{WO}_3$  plays a major role in the contribution of electrochromic performance of the ECD [2,5,15]. In addition, the CV area after 1000 cycles is slightly smaller than that after 10 cycles, suggesting that the active units involved in the electrochromic reaction in ECD are slightly reduced owing to the ion-trapping effect in the  $\text{NiO}$  and  $\text{WO}_3$  layers [31,32]. More importantly, it is noted that the current density of CV curves in the high potential range ( $>0.25$  V) is close to 0, implying that the leakage current of this ECD is extremely small, and this also reflects that the 300 nm thick  $\text{TaO}_x$  film prepared at an  $\text{Ar}/\text{O}_2$  ratio of 30/4 can effectively block the flow of electrons inside the ECD.

Figure 10b exhibits the transmittance spectra of the ECD in the bleached state ( $T_b$ ) and colored state ( $T_c$ ) and transmittance modulation ( $\Delta T = T_b - T_c$ ) in the 10th cycle and 1000th cycle. The voltages of  $-1.5$  V and  $1$  V were applied to the coloring process and bleaching process of ECD, respectively. As observed, the ECD exhibits a relatively high bleaching transmittance in the visible region and has a transmittance of 82% at 550 nm, which is sensitive to human eyes, showing a transparent feature. Moreover, at the 10th cycle, the ECD have a  $\Delta T$  of 42% at 550 nm and a maximum  $\Delta T$  of 46.3% at 668 nm. After 1000 cycles, the  $\Delta T$  of ECD at 550 nm and 668 nm still remain at 34.1% and 37%, respectively, indicating good optical modulation characteristics of the ECD.

Response time is defined as the time needed to reach 90% of the transmittance modulation  $\Delta T$  of the ECD at a fixed wavelength. Figure 10c displays the in situ transmittance curves of the ECD after 10 and 1000 cycles at 550 nm. It can be seen that the ECD after 10 cycles has a short response time of 8.9 s for coloring and 1.7 s for bleaching. A short response time for an ECD requires faster ion diffusion and higher ion conductivity. Generally speaking, the color/bleaching response time of all-solid-state ECD is more than 10 s due to the low ion diffusion rate in the solid electrolyte [6]. The faster response speed in this work could be attributed to the low relative density and porous and loose structure of the  $\text{TaO}_x$  electrolyte film, which leads to faster ion migration by surface conduction [20]. This is also supported by Xie et al., who realized a fast response (coloring 5.7 s; bleaching 2.2 s) through the loose  $\text{Li}_x\text{AlO}_z$  electrolyte film structure used in all-solid-state ECDs [6]. After 1000 cycles, the bleaching response time of ECD do not change significantly compared with the initial stage, while the coloring time becomes longer, which is 18.8 s. It has been reported that the active  $\text{Li}^+$  ions in the cycle process will be partially trapped in the  $\text{WO}_3$  and  $\text{NiO}$

layer, which is difficult to escape, and the ion-trapping in the NiO layer is dominant [31,32]. Furthermore, the trapping of  $\text{Li}^+$  ions results in larger transfer resistance and smaller charge diffusion coefficient [15,33], which hinders the transfer kinetics of ions between the  $\text{WO}_3$  and NiO layer, especially the transfer from the NiO to  $\text{WO}_3$  layer. As a result, the coloring time becomes longer after a long cycle. In addition, the obvious difference between bleaching time and coloring time could be related with the relatively higher electron conductivity for colored both NiO and  $\text{WO}_3$  layers, leading to a faster bleaching response [34,35].

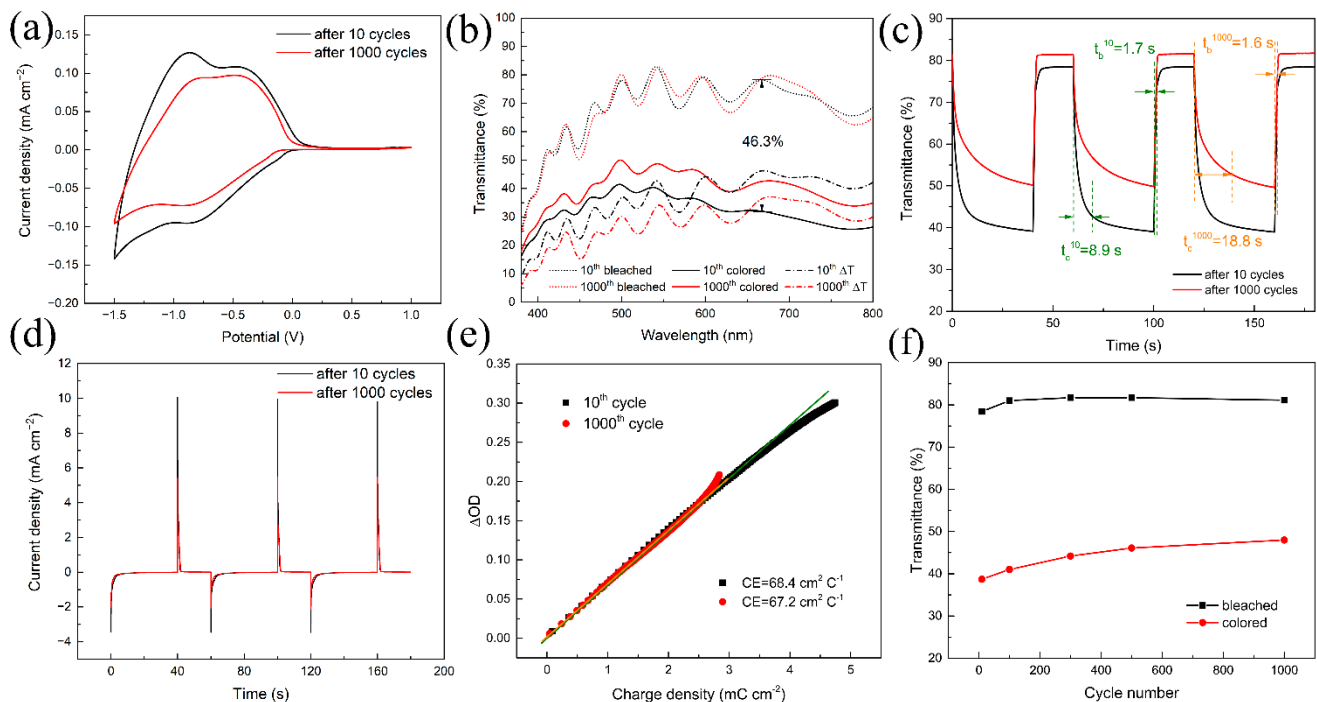


**Figure 10.** The electrochemical and EC performance of all-solid-state ECD. (a) CV curves of the all-solid-state ECD after 10 cycles and 1000 cycles; (b) Optical transmittance spectra of the colored state, bleached state and transmittance modulation  $\Delta T$ ; (c) In situ transmittance measurements at 550 nm performed at  $-1.5$  V for 40 s and 1 V for 20 s; (d) Current density–time curves corresponding to (c); (e) Optical density vs. charge density of the ECD at 550 nm; and (f) Cyclic stability of the ECD.

Figure 10d shows the corresponding current density–time curves to present the rapid migration and charge capacity in the ECD. Obviously, the fast coloring/bleaching response can be observed. Due to the relatively higher electronic conductivity of the colored  $\text{WO}_3$  and NiO films, the peak current density during bleaching is greater than that during coloring. Compared with the ECD after 10 cycles, the peak current density of the ECD after 1000 cycles is smaller for both the coloring and bleaching processes due to the reduction in active  $\text{Li}^+$  ions. Further, most importantly, the ECD has a very small residual current density in the balanced state, namely the leakage current, whether in the coloring or bleaching process. Under the conditions of  $-1.5$  V for 40 s and 1 V for 20 s, the leakage current of the ECD after 10 and 1000 cycles is  $3.3$  and  $4.4 \mu\text{A cm}^{-2}$  during coloring and  $14.5$  and  $12.6 \mu\text{A cm}^{-2}$  during bleaching, respectively. Such small leakage currents prove the strong electron blocking ability of the  $\text{TaO}_x$  film prepared in this study, which is consistent with the results of the CV curves in Figure 10a.

Coloration efficiency (CE) is also a significant criterion to evaluate the performance of the ECD, which can be determined by the change of optical density ( $\Delta OD$ ) per unit charge density ( $\Delta Q$ ); it can be calculated by the following equations:  $\text{CE} = \Delta OD / \Delta Q = \log(T_b / T_c) / \Delta Q$ , where the  $\Delta OD$  and  $\Delta Q$  were calculated from the in situ transmittance and the corresponding CA curves at 550 nm in Figure 10c,d. The CE values were calculated from the slope of the fitting line of  $\Delta OD$  versus  $\Delta Q$ , as shown in Figure 10e. It can be

observed that the CE value of ECD in 10th cycle is up to  $68.4 \text{ cm}^2 \text{ C}^{-1}$ , which is comparable to or even higher than the values reported in the literature [3,6,8,36]. Even after 1000 cycles, when the optical density decreases slightly, the CE value of the ECD still remains as high as  $67.2 \text{ cm}^2 \text{ C}^{-1}$ . The high CE values suggest that the ECD could obtain large optical modulation with small changes of inserted charges.

Figure 10f further shows the change trend of the transmittance of ECD in the colored/bleached state during the cycle. As observed, after the initial activation stage, the transmittance in the bleached state of ECD remained stable with the increase in the number of cycles. Further, the transmittance in the colored state first increased slightly and then gradually stabilized. After 1000 cycles, the ECD still has 81.2% retention rate of initial optical modulation and the same cross-sectional morphology (Figure S3) as Figure 9b, showing good cycle stability of the all-solid-state ECD. In addition, it can be easily acquired from the foregoing that the ion-trapping in the NiO layer is mainly responsible for the slight increase in the transmittance of the colored state. The enhancement of the stability of NiO layer can be achieved by element doping [37,38] or construction of special structures [39] in future work.

#### 4. Conclusions

In this work, the optical and electrochemical properties of  $\text{TaO}_x$  electrolyte film deposited by reactive p-DC magnetron sputtering were systematically investigated for application in the ECDs. All  $\text{TaO}_x$  films reactively sputtered in different Ar/O<sub>2</sub> ratios were amorphous. The surface morphology, roughness, O/Ta atomic ratio, optical band gap, refractive index, and relative density of the  $\text{TaO}_x$  film were found to be closely related to the Ar/O<sub>2</sub> ratio introduced during sputtering. The surface morphology of the films has columnar particle clusters with a porous and loose structure, separated by void boundaries. With the increase in oxygen flux, the porosity and surface roughness of the film gradually increase, the O/Ta atomic ratio gradually approaches the stoichiometric ratio, the optical band gap gradually increases, and the refractive index and relative density gradually decrease. Furthermore, the electronic conductivity of the  $\text{TaO}_x$  film decreases with the increase in oxygen flux owing to the reduction in oxygen vacancies. The low electronic conductivities of the order of  $10^{-12} \text{ S cm}^{-1}$  were obtained in the  $\text{TaO}_x$  films with Ar/O<sub>2</sub> ratio of 30/4 and 30/5. The electrochemical and optical measurement results of ITO/WO<sub>3</sub>/TaO<sub>x</sub> show that the ion conduction ability of the  $\text{TaO}_x$  film is also enhanced with the increase in oxygen content, which could be attributed to the loose structure of the  $\text{TaO}_x$  film, providing fast channels for ion conduction by surface. A multilayered inorganic all-solid-state ECD with the configuration of glass/ITO/WO<sub>3</sub>/Li/TaO<sub>x</sub>/NiO/ITO was prepared by the magnetron sputtering method. Under the driving voltage of  $-1.5 \text{ V}/1 \text{ V}$ , the ECD exhibited considerable optical modulation (46.3% at 668 nm), high coloring efficiency ( $68.4 \text{ cm}^2 \text{ C}^{-1}$ ), a fast response speed (8.9 s for coloring and 1.7 s for bleaching), and good cycle stability. In addition, the ECD has a much lower leakage current density due to the outstanding electron blocking ability of the  $\text{TaO}_x$  electrolyte layer.

**Supplementary Materials:** The following supporting information can be downloaded at: <https://www.mdpi.com/article/10.3390/coatings12121831/s1>, Figure S1: Optical transmittance spectra and corresponding digital photos of ITO/WO<sub>3</sub> and ITO/WO<sub>3</sub>/Li. Figure S2: XRD patterns of NiO, WO<sub>3</sub>/Li and WO<sub>3</sub> films on silica glass substrates. Figure S3: The cross-sectional morphology of the ECD after 1000 cycles.

**Author Contributions:** Conceptualization, J.L. and Y.Y.; methodology, J.L. and W.L.; investigation, J.L., W.L. and Y.W.; writing—original draft preparation, J.L.; writing—review and editing, W.L. and Y.W.; supervision, W.L.; project administration, Y.W.; funding acquisition, Y.Y. All authors have read and agreed to the published version of the manuscript.

**Funding:** This study is financially supported by BAIMTEC MATERIAL CO., LTD (No. ZC00TM2104).

**Institutional Review Board Statement:** Not applicable.

**Informed Consent Statement:** Not applicable.

**Data Availability Statement:** The authors confirm that the data supporting the findings of this study are available within the article.

**Conflicts of Interest:** The authors declare no conflict of interest.

## References

1. Wang, Z.; Wang, X.; Cong, S.; Geng, F.; Zhao, Z. Fusing electrochromic technology with other advanced technologies: A new roadmap for future development. *Mater. Sci. Eng. R Rep.* **2020**, *140*, 100524. [[CrossRef](#)]
2. Chen, X.; Dou, S.; Li, W.; Liu, D.; Zhang, Y.; Zhao, Y.; Li, Y.; Zhao, J.; Zhang, X. All solid state electrochromic devices based on the LiF electrolyte. *Chem. Commun.* **2020**, *56*, 5018–5021. [[CrossRef](#)] [[PubMed](#)]
3. Chen, X.; Zhang, H.; Li, W.; Xiao, Y.; Zhang, X.; Li, Y. CaF<sub>2</sub>: A novel electrolyte for all solid-state electrochromic devices. *Environ. Sci. Ecotechnol.* **2022**, *10*, 100164. [[CrossRef](#)]
4. Wang, R.; Pan, L.; Han, Q.; Zhu, H.; Wan, M.; Mai, Y. Reactively sputtered Ta<sub>2</sub>O<sub>5</sub> solid electrolyte layers in all thin film electrochromic devices. *J. Alloys Compd.* **2021**, *865*, 158931. [[CrossRef](#)]
5. Xiao, Y.; Dong, G.; Guo, J.; Liu, Q.; Huang, Q.; Zhang, Q.; Zhong, X.; Diao, X. Thickness dependent surface roughness of sputtered Li<sub>2.5</sub>TaO<sub>x</sub> ion conductor and its effect on electro-optical performance of inorganic monolithic electrochromic device. *Sol. Energy Mater. Sol. Cells* **2018**, *179*, 319–327. [[CrossRef](#)]
6. Xie, L.; Zhao, S.; Zhu, Y.; Zhang, Q.; Chang, T.; Huang, A.; Jin, P.; Ren, S.; Bao, S. High performance and excellent stability of all-solid-state electrochromic devices based on a Li<sub>1.85</sub>AlO<sub>2</sub> ion conducting layer. *ACS Sustain. Chem. Eng.* **2019**, *7*, 17390–17396. [[CrossRef](#)]
7. Li, J.; Wei, Y.; Liu, W.; Luo, J.; Yan, Y. High performance inorganic all-solid-state electrochromic devices based on Si<sub>3</sub>N<sub>4</sub> ion conducting layer. *Sol. Energy Mater. Sol. Cells* **2023**, *250*, 112073. [[CrossRef](#)]
8. Zhao, Y.; Zhang, X.; Chen, X.; Li, W.; Li, Z.; Chen, M.; Sun, W.; Zhao, J.; Li, Y. All-solid-state electrochromic devices based on the LiAlSiO<sub>4</sub> electrolyte. *Mater. Lett.* **2021**, *292*, 129592. [[CrossRef](#)]
9. Ashrit, P.V.; Girouard, F.E.; Truong, V.-V.; Bader, G. LiF as electrolyte for solid state electrochromic structures. *Opt. Mater. Technol. Energy Effic. Sol. Energy Convers. IV* **1985**, *562*, 53–61.
10. Corbella, C. Influence of the porosity of RF sputtered Ta<sub>2</sub>O<sub>5</sub> thin films on their optical properties for electrochromic applications. *Solid State Ion.* **2003**, *165*, 15–22. [[CrossRef](#)]
11. Tajima, K.; Yamada, Y.; Bao, S.; Okada, M.; Yoshimura, K. Electrochemical evaluation of Ta<sub>2</sub>O<sub>5</sub> thin film for all-solid-state switchable mirror glass. *Solid State Ion.* **2009**, *180*, 654–658. [[CrossRef](#)]
12. Saito, T.; Ushio, Y.; Yamada, M.; Niwa, T. Properties of tantalum oxide thin film for solid electrolyte. *Solid State Ion.* **1990**, *40–41*, 499–501. [[CrossRef](#)]
13. Duggan, M.J.; Saito, T.; Niwa, T. Ionic conductivity of tantalum oxide by rf sputtering. *Solid State Ion.* **1993**, *62*, 15–20. [[CrossRef](#)]
14. Gismatulina, A.; Gritsenko, V.; Perevalov, T.; Kuzmichev, D.; Chernikova, A.; Markeev, A. Charge transport mechanism in atomic layer deposited oxygen-deficient TaO<sub>x</sub> Films. *Phys. Status Solidi B* **2020**, *258*, 2000432. [[CrossRef](#)]
15. Liu, Q.; Dong, G.; Chen, Q.; Guo, J.; Xiao, Y.; Delplancke-Ogletree, M.-P.; Reniers, F.; Diao, X. Charge-transfer kinetics and cyclic properties of inorganic all-solid-state electrochromic device with remarkably improved optical memory. *Sol. Energy Mater. Sol. Cells* **2018**, *174*, 545–553. [[CrossRef](#)]
16. Li, W.; Zhang, X.; Chen, X.; Zhao, Y.; Wang, L.; Chen, M.; Zhao, J.; Li, Y.; Zhang, Y. Effect of independently controllable electrolyte ion content on the performance of all-solid-state electrochromic devices. *Chem. Eng. J.* **2020**, *398*, 125628. [[CrossRef](#)]
17. Han, Q.; Wang, R.; Zhu, H.; Wan, M.; Mai, Y. The preparation and investigation of all thin film electrochromic devices based on reactively sputtered MoO<sub>3</sub> thin films. *Mater. Sci. Semicond. Process.* **2021**, *126*, 105686. [[CrossRef](#)]
18. Ngaruiya, J.M.; Kappertz, O.; Mohamed, S.H.; Wuttig, M. Structure formation upon reactive direct current magnetron sputtering of transition metal oxide films. *Appl. Phys. Lett.* **2004**, *85*, 748–750. [[CrossRef](#)]
19. Berg, S.; Särhammar, E.; Nyberg, T. Upgrading the “Berg-model” for reactive sputtering processes. *Thin Solid Films* **2014**, *565*, 186–192. [[CrossRef](#)]
20. Liu, Z.; Fu, W.; Payzant, E.A.; Yu, X.; Wu, Z.; Dudney, N.J.; Kiggans, J.; Hong, K.; Rondinone, A.J.; Liang, C. Anomalous high ionic conductivity of nanoporous β-Li<sub>3</sub>PS<sub>4</sub>. *J. Am. Chem. Soc.* **2013**, *135*, 975–978. [[CrossRef](#)] [[PubMed](#)]
21. Li, J.; Liu, Y.; Zhu, Z.; Zhang, G.; Zou, T.; Zou, Z.; Zhang, S.; Zeng, D.; Xie, C. A full-sunlight-driven photocatalyst with super long-persistent energy storage ability. *Sci. Rep.* **2013**, *3*, 2409. [[CrossRef](#)]
22. ISO 9050; Glass in Building—Determination of Light Transmittance, Solar Direct Transmittance, Total Solar Energy Transmittance and Ultraviolet Transmittance, and Related Glazing Factors. International Organization for Standardization: Geneva, Switzerland, 1990.
23. Deb, S.K. A novel electrophotographic system. *Appl. Opt.* **1969**, *8*, 192–195. [[CrossRef](#)]
24. Saleem, M.; Al-Kuhaili, M.F.; Durrani, S.M.A.; Hendi, A.H.Y.; Bakhtiari, I.A.; Ali, S. Influence of hydrogen annealing on the optoelectronic properties of WO<sub>3</sub> thin films. *Int. J. Hydrogen Energy* **2015**, *40*, 12343–12351. [[CrossRef](#)]
25. Swanepoel, R. Determination of the thickness and optical constants of amorphous silicon. *J. Phys. E Sci. Instrum.* **1983**, *16*, 1214. [[CrossRef](#)]
26. Heitmann, W. Vacuum evaporated films of aluminum fluoride. *Thin Solid Films* **1970**, *1*, 61–67. [[CrossRef](#)]

27. Franke, E.; Trimble, C.L.; DeVries, M.J.; Woollam, J.A.; Schubert, M.; Frost, F. Dielectric function of amorphous tantalum oxide from the far infrared to the deep ultraviolet spectral region measured by spectroscopic ellipsometry. *J. Appl. Phys.* **2000**, *88*, 5166–5174. [[CrossRef](#)]
28. Fleming, R.M.; Lang, D.V.; Jones, C.D.W.; Steigerwald, M.L.; Murphy, D.W.; Alers, G.B.; Wong, Y.-H.; Dover, R.B.v.; Kwo, J.R.; Sergent, A.M. Defect dominated charge transport in amorphous Ta<sub>2</sub>O<sub>5</sub> thin films. *J. Appl. Phys.* **2000**, *88*, 850–862. [[CrossRef](#)]
29. Kitao, M.; Akram, H.; Urabe, K.; Yamada, S. Properties of solid-state electrochromic cells using Ta<sub>2</sub>O<sub>5</sub> as electrolyte. *J. Electron. Mater.* **1992**, *21*, 419–422. [[CrossRef](#)]
30. Li, W.; Zhang, X.; Chen, X.; Zhao, Y.; Wang, L.; Chen, M.; Li, Z.; Zhao, J.; Li, Y. Lithiation of WO<sub>3</sub> films by evaporation method for all-solid-state electrochromic devices. *Electrochim. Acta* **2020**, *355*, 136817. [[CrossRef](#)]
31. Dong, D.; Wang, W.; Rougier, A.; Dong, G.; Da Rocha, M.; Presmanes, L.; Zrikem, K.; Song, G.; Diao, X.; Barnabe, A. Life-cycling and uncovering cation-trapping evidence of a monolithic inorganic electrochromic device: Glass/ITO/WO<sub>3</sub>/LiTaO<sub>3</sub>/NiO/ITO. *Nanoscale* **2018**, *10*, 16521–16530. [[CrossRef](#)]
32. Dong, D.; Wang, W.; Rougier, A.; Barnabé, A.; Dong, G.; Zhang, F.; Diao, X. Lithium trapping as a degradation mechanism of the electrochromic properties of all-solid-state WO<sub>3</sub>/NiO devices. *J. Mater. Chem. C* **2018**, *6*, 9875–9889. [[CrossRef](#)]
33. Bisquert, J. Analysis of the kinetics of ion intercalation: Ion trapping approach to solid-state relaxation processes. *Electrochim. Acta* **2002**, *47*, 2435–2449. [[CrossRef](#)]
34. Wang, Z.; He, Y.; Gu, M.; Du, Y.; Mao, S.X.; Wang, C. Electron transfer governed crystal transformation of tungsten trioxide upon Li ions intercalation. *ACS Appl. Mater. Interfaces* **2016**, *8*, 24567–24572. [[CrossRef](#)]
35. Soo Kim, D.; Chul Lee, H. Nickel vacancy behavior in the electrical conductance of nonstoichiometric nickel oxide film. *J. Appl. Phys.* **2012**, *112*, 034504. [[CrossRef](#)]
36. Liu, Q.; Dong, G.; Xiao, Y.; Gao, F.; Wang, M.; Wang, Q.; Wang, S.; Zuo, H.; Diao, X. An all-thin-film inorganic electrochromic device monolithically fabricated on flexible PET/ITO substrate by magnetron sputtering. *Mater. Lett.* **2015**, *142*, 232–234. [[CrossRef](#)]
37. Wen, R.T.; Niklasson, G.A.; Granqvist, C.G. Strongly improved electrochemical cycling durability by adding iridium to electrochromic nickel oxide films. *ACS Appl. Mater. Interfaces* **2015**, *7*, 9319–9322. [[CrossRef](#)] [[PubMed](#)]
38. Lee, S.J.; Lee, T.-G.; Nahm, S.; Kim, D.H.; Yang, D.J.; Han, S.H. Investigation of all-solid-state electrochromic devices with durability enhanced tungsten-doped nickel oxide as a counter electrode. *J. Alloys Compd.* **2020**, *815*, 152399. [[CrossRef](#)]
39. Hou, S.; Zhang, X.; Tian, Y.; Zhao, J.; Geng, H.; Qu, H.; Zhang, H.; Zhang, K.; Wang, B.; Gavriluk, A.I.; et al. Improved electrochemical cycling durability in a nickel oxide double layer film. *Chem.—Asian J.* **2017**, *12*, 2922–2928. [[CrossRef](#)]